Symmetric Airy beams

Pablo Vaveliuk,[1,2,*] Alberto Lencina,[2,3] Jose A. Rodrigo,[4] and Oscar Martinez Matos[4]

[1]*Faculdade de Tecnologia, Servicio Nacional de Aprendizagem Industrial SENAI-Cimatec Av. Orlando Gomes 1845 41650-010, Salvador, Bahia, Brazil*

[2]*Centro de Investigaciones Ópticas (CICBA-CONICET), Cno. Parque Centenario s/n 1897 Gonnet, La Plata, Pcia. de Buenos Aires, Argentina*

[3]*Departamento de Física, Fac. de Cs. Exactas, Universidad Nacional de La Plata, c.c. 67, 1900 La Plata, Pcia. de Buenos Aires, Argentina*

[4]*Departamento de Óptica, Facultad de Ciencias Físicas, Universidad Complutense de Madrid Av. Complutense s/n 28040 Madrid, Spain*

**Corresponding author: pvaveliu@fis.ucm.es*

Received December 27, 2013; revised March 12, 2014; accepted March 12, 2014; posted March 13, 2014 (Doc. ID 203843); published April 9, 2014

In this Letter a new class of light beam arisen from the symmetrization of the spectral cubic phase of an Airy beam is presented. The symmetric Airy beam exhibits peculiar features. It propagates at initial stages with a single central lobe that autofocuses and then collapses immediately behind the autofocus. Then, the beam splits into two specular off-axis parabolic lobes like those corresponding to two Airy beams accelerating in opposite directions. Its features are analyzed and compared to other kinds of autofocusing beams; the superposition of two conventional Airy beams having opposite accelerations (in rectangular coordinates) and also to the recently demonstrated circular Airy beam (in cylindrical coordinates). The generation of a symmetric Airy beam is experimentally demonstrated as well. Besides, based on its main features, some possible applications are also discussed.

OCIS codes: (140.3300) Laser beam shaping; (260.0260) Physical optics; (070.2580) Paraxial wave optics; (350.5500) Propagation.

http://dx.doi.org/10.1364/OL.39.002370

Since the demonstration of the so-called accelerating Airy beam [1,2] in 2007, the research related to these peculiar self-bending beams has grown quickly, so much in basic research [3] as in its generation, control, and applications [4]. Nowadays, it constitutes an important research area of optical beam propagation and design [5]. This beam is a separable solution of the Helmholtz equation in the paraxial regime for rectangular coordinates, and therefore, it can be generated in one or two transverse dimensions. Its field profile is an exponentially modulated Airy function being, a square-integrable profile encompassing a finite energy content. The Airy function has no defined symmetry in rectangular coordinates, but if extended to cylindrical ones, it results in a beam having circular symmetry with an Airy radial profile, called abruptly autofocusing beam or circular Airy beam (CAB) [6–8]. These beams were experimentally demonstrated [9,10] and possess an unusual feature. As they propagate the profile is accelerated toward the center of symmetry yielding a parabolic caustic surface of revolution. This surface collapses on axis to an autofocus with high intensity. This autofocus is a consequence of the optical field structure itself, and not by any nonlinear effect. The research on CABs has grown quickly in the last years, encouraged by the potential applications in laser medicine, laser ablation, and other linear or nonlinear optical settings [11].

CABs are necessarily two-dimensional transverse structures since they were conceived as radially symmetric beams in cylindrical coordinates. A main question for Airy-type structures concerns the possible link: *circular symmetry* ↔ *autofocusing properties*. Indeed, the extension of the Airy beam design to the cylindrical frame compels the resulting beam to acquire a radial symmetry. And this symmetry that allows the appearance of autofocusing features. Nevertheless, the rectangular coordinates represent the natural symmetry of a conventional Airy beam. Then, is it feasible an Airy-like beam with autofocusing characteristics in a rectangular frame? We underline that the superposition of two Airy beams, having opposite accelerations and having their principal lobes mostly overlapped, yields an autofocusing structure. Such a beam, called dual Airy beam (DAB), has been recently analyzed [12], although its autofocusing properties were not considered in that work. However, even if a manipulation of a DAB is theoretically possible, in practice, the experimental generation of two independent Airy beams overlapped in a fashion to obtain a DAB exhibiting autofocusing properties seems to be an extremely complex technical task.

In this Letter we develop a formalism to generate an Airy beam having rectangular symmetry and autofocusing properties that can be experimentally created as easily as a conventional Airy beam. Mathematically, this symmetric Airy beam (SAB) arises from a finite-energy Airy beam by only changing the odd parity by the even parity in its spectral cubic phase. We perform a numerical analysis showing its main properties. Besides, the SAB is compared with other kinds of autofocusing Airy-like beams such as DABs and CABs, and possible applications are also discussed. Finally, we experimentally demonstrate the generation of a symmetric Airy beam.

A key feature of a finite-energy Airy beam is the relationship between its initial profile (ip) in the coordinate space x, its Gaussian amplitude (Ga), and cubic phase (cp) in the spectral (conjugate) space K. At the initial stage of propagation $z = 0$, the Fourier transform of the spatial field $u(x, 0) = u_0$ is the spectral field $\mathfrak{U}(K, 0) = \mathfrak{U}_0 \equiv \mathcal{F}\{u_0\}$, where $\mathcal{F}$ is the Fourier transform

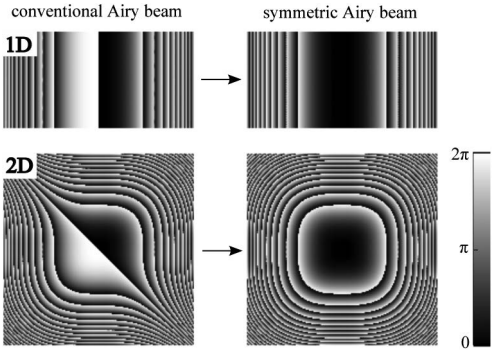

Fig. 1. 1D and 2D wrapped spectral phase masks for a conventional Airy beam and for the resulting SAB when the phase parity is changed. The unwrapped phase ranges corresponds to $[-20\pi, 20\pi]$.

operator. Both conjugate fields are explicitly given by [13]:

$$u_0 = \underbrace{e^{\frac{ax}{x_0}}\mathrm{Ai}(x/x_0)}_{ip} \rightleftharpoons \mathfrak{U}_0 = x_0 e^{\frac{a^3}{3}} \underbrace{e^{-aK^2x_0^2}}_{\mathrm{Ga}} \underbrace{e^{\frac{iK^3x_0^3}{3}}}_{\mathrm{cp}} e^{iKa^2x_0}, \quad (1)$$

where x_0 accounts for the size of the Airy central lobe, and the parameter $a > 0$ is the exponential truncation factor that guarantees the square integrability of the beam and controls its spreading properties [1,14]. The linear phase term $\exp(iKa^2x_0)$ has no real effect in the beam properties for the range of a where the self-bending dynamic dominates ($a \ll 1$) and in practice, is not considered. The SAB is obtained by only changing the parity in the spectral cubic phase, i.e., $K^3x_0^3/3 \to |K|^3x_0^3/3$, resulting in the one-dimensional (1D) and two-dimensional (2D) wrapped phase masks shown in Fig. 1. In this way, the beam intensity and spatial phase are even functions of the transverse spatial coordinate x. An analytic expression for an SAB was not found. However, its paraxial solution $v(x,z)$ can easily be built by using the angular spectrum formalism [15]

$$v(\tilde{x},\tilde{z}) = \left(\frac{1}{2\pi}\right)\int_{-\infty}^{+\infty} \underbrace{\mathfrak{V}_0 e^{i2\pi\tilde{z}[1-\tilde{K}^2/(8\pi^2)]}}_{\mathfrak{V}(\tilde{K},\tilde{z})} e^{i\tilde{K}\tilde{x}}\mathrm{d}\tilde{K}, \quad (2)$$

where $\mathfrak{V}(\tilde{K},\tilde{z}) \equiv \mathcal{F}\{v(\tilde{x},\tilde{z})\}$ and the even cubic phase enters the argument of $\mathfrak{V}_0$:

$$\mathfrak{V}_0 = \mathfrak{V}(\tilde{K},0) = \tilde{x}_0 e^{a^3/3} e^{-a\tilde{K}^2\tilde{x}_0^2} e^{i|\tilde{K}|^3\tilde{x}_0^3/3} \equiv \mathcal{F}\{v_0\}. \quad (3)$$

Dimensionless variables and parameters ($\tilde{z} = z/\lambda$, $\tilde{x} = x/\lambda$, $\tilde{x}_0 = x_0/\lambda$, $\tilde{K} = \lambda K$, being λ the wavelength) are used to simplify the numerical integration of Eq. (2), but for a more comprehensive interpretation, the figures are depicted in terms of the current transverse and longitudinal parameters often used in Airy beam literature, $s = x/x_0$ and $\xi = \lambda z/(2\pi x_0^2)$. Figure 2(a) shows the intensity distribution of a 1D SAB, $I_v \equiv |v|^2$, as a function of (s,ξ) and Figs. 2(b)–2(f) show intensity patterns of a 2D SAB as a function of transverse spatial variables (s_x, s_y) for several planes $\xi = \text{const}$. Notice that the beam

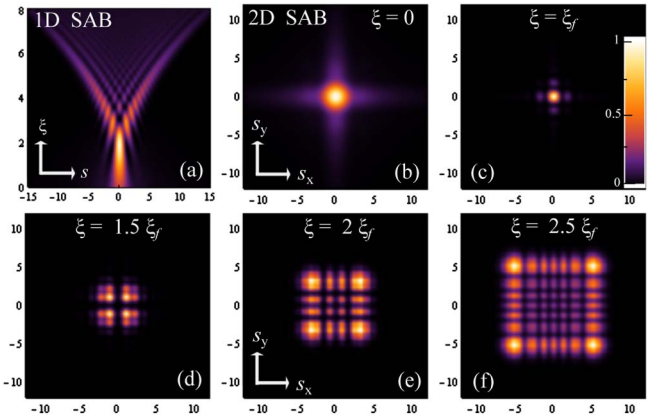

Fig. 2. (a) Intensity distribution for a 1D symmetric Airy beam versus (s,ξ). The intensity scale $[0,1]$ corresponds to $[0, I_v^f]$. (b)–(f) Intensity patterns for a 2D SAB as a function of (s_x, s_y) for several planes $\xi_i = 0, \xi_f, 1.5\xi_f, 2\xi_f, 2.5\xi_f$, ξ_f being the distance between the initial plane and the autofocus plane. The intensity scale $[0,1]$ for each 2D pattern corresponds to $[0, I_v^{\max}(\xi_i)]$. All these intensity distributions were obtained by numerical integration of Eq. (2).

energy is mostly concentrated in a single central lobe during the initial stages of propagation. The maximum intensity, or peak intensity as a function of ξ, i.e., $I_v^{\max} \equiv I_v^{\max}(\xi)$, rapidly increases as ξ increases up to reach its extreme value at the *autofocus*, located at $\xi = \xi_f$. We name the intensity of the SAB at autofocus by $I_v^f \equiv I_v^{\max}(\xi_f)$. For the parameters used in the simulations $\tilde{x}_0 = 100$ and $a = 0.08$, it has $\xi_f \approx 1.9$ for both 1D and 2D cases. For $\xi > \xi_f$, $I_v^{\max}$ quickly decreases as ξ increases so that the *on-axis* lobe collapses just after the autofocus. At this stage, the beam splits into two specularly symmetric *off-axis* lobes whose peak intensity follows a parabolic trajectory, which resembles those lobes corresponding to two conventional Airy beams accelerating in opposite directions. This is clearly observed in Fig. 2(a) for the 1D case. For the 2D case, the central lobe becomes, after collapsing, four off-axis identical lobes with the peak intensity following parabolic trajectories on the planes $x = \pm y$ and moving away from the optical axis (z axis) as the beam propagates. In Figs. 2(b)–2(f), the intensity pattern at each plane $\xi = \xi_i$ was normalized to the peak intensity on its own plane, i.e., $I_v^{\max}(\xi_i)$, and not to the intensity at autofocus, I_v^f. This is to help the visualization of the beam pattern structure on each transverse plane. Notice that behind the autofocus, the beam pattern evolves from an internal vertex of peak intensity at $\xi = 1.5\xi_f$ to an external vertex at $\xi = 2\xi_f$ in a square symmetry.

On the other hand, and for comparative purposes, we study the DAB. This beam is a superposition of the complex fields of two conventional Airy beams, u_+ and u_-, each one accelerating in an opposite direction of x, respectively. Mathematically, the DAB intensity takes the form $I_d = |u_+(s,\xi) + u_-(s,\xi)|^2$. Figure 3(a) shows the intensity distribution for a 1D DAB as a function of (s,ξ). The intensity is normalized to the peak intensity of an SAB at the autofocus, i.e., I_d/I_v^f. Figures 3(b)–3(f) show intensity patterns for a 2D DAB normalized to the maximum intensity of an SAB at each plane $\xi = \xi_i$, i.e.,

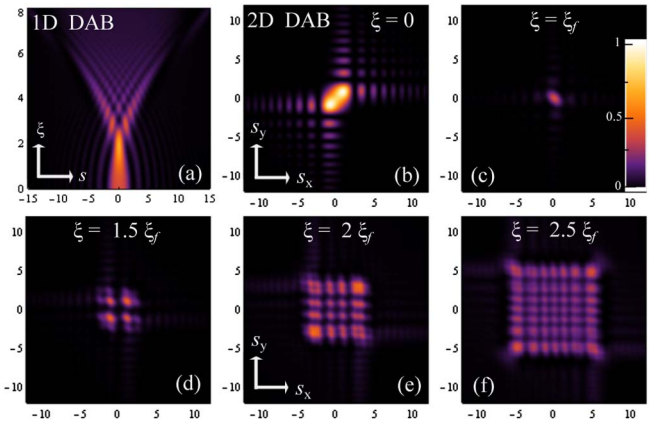

Fig. 3. (a) Intensity distribution for a 1D dual Airy beam (DAB) versus (s,ξ). The intensity scale $[0,1]$ corresponds to $[0,I_v^f]$. (b)–(f) Intensity patterns for a 2D DAB versus (s_x,s_y) at the planes $\xi_i=0$, ξ_f, $1.5\xi_f$, $2\xi_f$, $2.5\xi_f$. The intensity scale $[0,1]$ corresponds to $[0,I_v^{\max}(\xi_i)]$. All these intensity distributions were obtained from the superposition of well-known analytical expressions for the Airy beam with opposite accelerations.

$I_d(\xi_i)/I_v^{\max}(\xi_i)$, as a function of (s_x,s_y). The autofocus for DABs in Fig. 3 is also located at $\xi=\xi_f$, and the energy content of such DABs was set to be equal to SABs of Fig. 2. There are qualitative resemblances between both beams. However, there are important quantitative differences. At ξ_f the DAB has 12% less energy concentrated in the central lobe Its peak intensity is 39% smaller and has a peak 60% wider than that corresponding to the SAB. Moreover, after ξ_f the DAB spreads in several secondary lobes while the SAB holds two main lobes that spread according to the central lobes of Airy beams for large ξ. Figure 4 depicts the maximum intensity (peak intensity) for symmetric, dual, and conventional Airy beams as a function of ξ. It is clear that SAB and DAB have approximately the same peak intensity at the initial stage of propagation $\xi=0$. But at $\xi=\xi_f$ the peak intensity is higher for SAB. For a 1D case, the ratio is $I_v^f/I_d^f\approx 1.5$, while this ratio is greater for the 2D case $I_v^f/I_d^f\approx 2.7$. On the other hand, for large ξ, $I_v^{\max}$ and $I_u^{\max}$ have identical behavior being both larger than $I_d^{\max}$. Thereby, the SAB has better nondiffracting properties if compared with the DAB. Furthermore, SABs are as easily realizable as a conventional Airy beam while DABs require an extremely complex experimental alignment task.

On the other hand, the only Airy-like beam with autofocusing properties experimentally demonstrated was the CAB [9,10], that only exists for two transverse

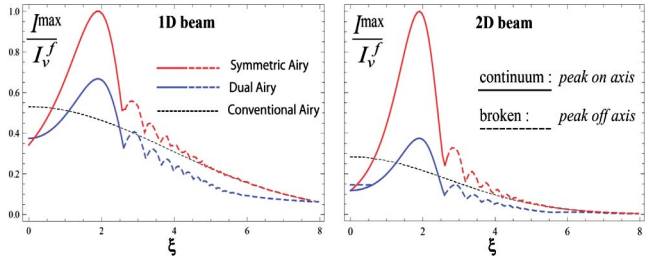

Fig. 4. Normalized peak intensity for SAB, $I_v^{\max}/I_v^f$, DAB $I_d^{\max}/I_v^f$, and conventional Airy beam $I_u^{\max}/I_v^f$ as a function of ξ.

dimensions because of its circular-cylindrical symmetry. One of the main characteristics of CABs is that the ratio autofocus/initial peak intensity can reach several orders of magnitude [6–8], while such a ratio is about one order of magnitude for a 2D SAB, as shown in Fig. 4. However, this should be not seen as a disadvantage for SABs since the propagation dynamics of both classes of beams is different. The CAB is initially formed as a succession of Airy rings being the inner ring, the principal one. This ring bends as propagates to a focal point on the axis of symmetry. After the autofocus, the energy is mostly concentrated in a central on-axis lobe as z increases (see for instance Fig. 2 in [7]). This process is *dynamically inverse* to what happens with SABs because, in this last case, the autofocus is generated from the central lobe while in the CAB case, the central lobe is a result of the beam collapse. This *inverse* propagation behavior of SABs with respect to CABs, in addition to their different spatial symmetries, lead to us to think that both beams may be seen as complementary for practical applications. SABs could also be useful in optical micromanipulation requiring symmetric Airy patterns as pointed out in [12]. In curved channels of plasma [16], the SAB seems to be promising since it presents bifurcation and high intensity contrast (autofocusing) without any nonlinear effect. Besides, an advantage in relation to CABs is that SABs can also exist in 1D as planar beams opening the chance of developing applications to plasmonics [17].

Finally, we demonstrate the experimental realization of an SAB. A great advantage is that it can be generated similarly to a conventional Airy beam. The beam's complex field amplitude $\mathfrak{V}_0$ in Eq. (3) was encoded as a phase-only computer generated hologram (CGH) following the approach reported in [18]. Note that, alternatively to the CGH, the SAB can also be generated by modulating a Gaussian beam with the corresponding even cubic phase function. In our case, the CGH was addressed into a programmable reflective LCoS-SLM (Holoeye PLUTO, 8-bit gray-level, pixel pitch of 8 μm and 1920×1080 pixels) calibrated for a 2π phase shift at the wavelength $\lambda=532$ nm and corrected from static aberrations as reported in [19]. To generate the SAB, the hologram was illuminated by a collimated laser beam ($\lambda=532$ nm) and then focused by a spherical convergent lens (focal length of 10 cm, N-BK7 glass). The beam propagation in the focal region of such a focusing lens has been measured by using an sCMOS camera (Hamamatsu, Orca Flash 4.0, 16-bit gray-level, pixel size of 6.5 μm) and stored as a video (Media 1). Specifically, we measured 240 intensity patterns in the range $z\in[0,20]$ mm, where $z=0$ coincides with the focal plane position of the focusing lens. We use dimensional variables to illustrate the real propagation range and beam-size values of the generated SAB. In Fig. 5(a) we show the beam profile in the x–z axes where the autofocus region and the off-axis lobes are clearly distinguished. The intensity patterns at the distance $z_i=0$, z_f, $1.5z_f$, $2z_f$, $2.5z_f$ are displayed in Figs. 5(b)–5(f) being $z_f=5.7$ mm, the distance between the initial and the autofocus planes. Notice that these experimental patterns are in good agreement with the theoretical ones displayed in Fig. 2. These results experimentally confirm the main features of an SAB.

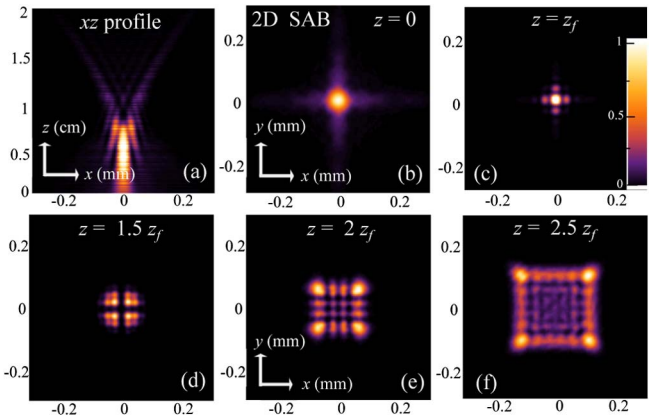

Fig. 5. (a) Experimental intensity profile on the xz plane for a 2D symmetric Airy beam versus (x, z). The intensity scale $[0, 1]$ corresponds to $[0, I_v^f]$. (b)–(f) Experimental intensity patterns for a 2D SAB as a function of (x, y) for different planes z_i. The density scale $[0, 1]$ for each 2D pattern corresponds to $[0, I_v^{\max}(z_i)]$. The SAB propagation from $z = 0$ to 20 mm is shown in Media 1.

In summary, a new class of Airy beams having rectangular symmetry and exhibiting autofocusing features was presented. The SAB arises from the symmetrization of the spectral cubic phase of a conventional Airy beam. The SAB can be generated in 1D and 2D as well. Its properties were analyzed and compared to those corresponding to other kinds of Airy-like autofocusing beams, DABs and CABs, and potential applications were discussed. The symmetric Airy beam was experimentally demonstrated in good agreement with the theoretical predictions. This new type of beam opens the possibility of studying different ways of trapping and guiding particles or using them to generate new structured plasma channels and waveguides in dielectric media as well as in plasmonic applications.

Financial support from the SENAI-DR/Bahia, Brazil, and the Spanish MEC under project TEC 2011-23629 is acknowledged. P. V. acknowledges a PQ fellowship from CNPq (Brazil).

References and Note

1. G. A. Siviloglou and D. N. Christodoulides, Opt. Lett. **32**, 979 (2007).
2. G. A. Siviloglou, J. Broky, A. Dogariu, and D. N. Christodoulides, Phys. Rev. Lett. **99**, 213901 (2007).
3. Y. Kaganovsky and E. Heyman, Opt. Express **18**, 8440 (2010).
4. Y. Hu, G. A. Siviloglou, P. Zhang, N. K. Efremidis, D. N. Christodoulides, and Z. Chen, in *Nonlinear Photonics and Novel Optical Phenomena*, Z. Chen and R. Morandotti, eds., Vol. **170** of Springer Series in Optical Sciences (Springer, 2013), pp. 1–46.
5. M. A. Bandres, I. Kaminer, M. S. Mills, B. M. Rodrguez-Lara, E. Greenfield, M. Segev, and D. N. Christodoulides, Opt. Phot. News **24**(6), 30 (2013).
6. N. K. Efremidis and D. N. Christodoulides, Opt. Lett. **35**, 4045 (2010).
7. I. D. Chremmos, N. K. Efremidis, and D. N. Christodoulides, Opt. Lett. **36**, 1890 (2011).
8. I. D. Chremmos, Z. Chen, D. N. Christodoulides, and N. K. Efremidis, Phys. Rev. A **85**, 023828 (2012).
9. D. G. Papazoglou, N. K. Efremidis, D. N. Christodoulides, and S. Tzortzakis, Opt. Lett. **36**, 1842 (2011).
10. I. D. Chremmos, P. Zhang, J. Prakash, N. K. Efremidis, D. N. Christodoulides, and Z. Chen, Opt. Lett. **36**, 3675 (2011).
11. P. Panagiotopoulos, D. G. Papazoglou, A. Couairon, and S. Tzortzakis, Nat. Commun. **4**, 2622 (2013).
12. Ch.-Y. Hwang, D. Choi, K.-Y. Kim, and B. Lee, Opt. Express **18**, 23504 (2010).
13. All the equations are given for one transverse dimension. However, the extension to two transverse dimensions is straightforward because of the rectangular symmetry.
14. I. M. Besieris and A. M. Shaarawi, Opt. Lett. **32**, 2447 (2007).
15. P. Vaveliuk and O. Martinez Matos, Opt. Express **20**, 26913 (2012).
16. J. Kasparian and J.-P. Wolf, J. Eur. Opt. Soc. (Rapid Publications) **4**, 09039 (2009).
17. A. Salandrino and D. N. Christodoulides, Physics **4**, 69 (2011).
18. J. A. Davis, D. M. Cottrell, J. Campos, M. J. Yzuel, and I. Moreno, Appl. Opt. **38**, 5004 (1999).
19. J. A. Rodrigo, T. Alieva, A. Cámara, O. Martínez-Matos, P. Cheben, and M. L. Calvo, Opt. Express **19**, 6064 (2011).